Int. J. Heat Mass Transfer. Vol. 22, pp. 469–483

0017-9310/79/0301-0469 $02.00/0

A STUDY OF TRANSPIRATION FROM POROUS FLAT PLATES SIMULATING PLANT LEAVES

JOSEPH N. CANNON,* WILLIAM B. KRANTZ and FRANK KREITH
Department of Chemical Engineering, University of Colorado, Boulder, Colorado 80302, U.S.A.

and

DAN NAOT†
Division of Fluid Mechanics and Heat Transfer, University of the Negev, Beer-Sheva, Israel

(*Received* 28 *June* 1977 *and in revised form* 22 *May* 1978)

Abstract—This article presents analytical models to predict the transpiration through perforated plates simulating the stomata of dicotyledon leaves under various flow conditions and compares the analytical predictions with experimental results. The analysis is based on fundamental concepts of boundary-layer theory and convective heat- and mass-transfer. The experiments were performed in an ecological wind tunnel with perforated plates resembling the stomatal geometry of broad leaves. Some unexpected anomalies in the results are explained by means of a turbulent penetration theory.

NOMENCLATURE

a, pore radius;
A_p, cross sectional area of a single pore;
A_t, total area of plate;
b, one half of average distance between axes of adjacent pores, see [37];
C, concentration;
d, pore diameter;
D, width of plate in y-direction;
$\mathcal{D}$, binary diffusivity;
e, turbulent energy;
f, penetration coefficient;
g, gravitational constant;
K, mass transfer coefficient;
L, length of plate in x-direction;
$\dot{m}$, mass flow rate;
N, number of pores;
$\dot{N}$, mass flux;
R, resistance;
s, center to center spacing between pores in flow direction;
t, thickness of plate, pore length;
T_c, temperature of water in the plate holder cavity;
$\overline{uv}$, Reynolds stress;
U, velocity in x-direction;
v', root mean square velocity fluctuation in z-direction;
v^*, friction velocity;
$\overline{vv}$, mean square velocity fluctuation in z-direction;
x, x', coordinates in direction of flow;
y, coordinate perpendicular to flow direction in plane of plate;
z, coordinate perpendicular to plate.

Greek symbols

δ, thickness of stagnant boundary layer;
μ, viscosity;
ρ, density;
τ_w, wall shear.

Dimensionless numbers

Gr, Grashof number;
Re, Reynolds number;
Sc, Schmidt number;
Sh, Sherwood number;
$\overline{Sh}_L$, Sherwood number, average for boundary layer based on $\bar{K}_{BL}$ and L.

Subscripts

A, water vapor;
BL, boundary layer;
E, effective;
i, inlet, substomatal cavity;
I, internal, pore and substomatal cavity (inlet);
L, based on length of plate;
O, outlet;
p, pore;
T, overall, total including boundary layer, pore, and substomatal cavity (inlet);
TP, turbulent penetration;
x, local;
∞, free stream.

Superscript

$\bar{}$, average based on length of plate.

*Presently Associate Professor and Chairman, Department of Chemical Engineering, Howard University, Washington, D.C. 20059, U.S.A.
†Authors are listed alphabetically.

I. INTRODUCTION

SINCE most of the water applied in irrigation is lost by transpiration, the water loss from the leaves of green plants is a process which has been of interest to botanists, ecologists, plant physiologists, and agricultural engineers for a long time. Transpiration from plants and agricultural eco-systems has received particular attention during the past decade, because it has been shown that probably as much as 80% of the water used by green plants is not really necessary for their physiological growth [1, 2] and that the water uptake of plants and trees can be reduced appreciably by various types of chemical antitranspirant sprays without causing any apparent physiological damage [3–6].

Nearly all the water evaporated by most plants passes through tiny openings in their leaves, called stomata. The shapes of stomatal passages vary considerably, but the stomatal openings in the leaf surface are approximately elliptical in shape, about 20 μm long, with the width varying from 1–10 μm. The stomatal passages serve simultaneously as the pathway for CO_2 entering the leaf from the atmosphere and for H_2O passing from the interior of the leaf into the atmosphere; their sizes are determined by the position of the two guard cells which surround each stoma. Typically, the density of stomata ranges from 7×10^7 to 6×10^8 stomata/m^2 of leaf surface, and, when fully open, it has been estimated that in broad-leaf plants, stomata occupy from 1 to 3% of the total surface area of the leaf. Detailed accounts of stomatal physiology are available in the literature [7, 8].

During the past ten years plant physiologists [9] have conducted many experimental investigations on broad-leaf plants in an effort to determine how air temperature, wind speed, solar radiation, and other environmental variables affect the opening and closing behavior of the stomata in the leaves, and how stomatal behavior is related to water consumption. In the interpretation of the experimental results it has generally been assumed [10] that the transpiration rate or mass transfer flux, $\dot{N}$, is directly proportional to the difference in the water vapor concentration between the interior of the leaf and its environment, ΔC, and inversely proportional to the sum of the internal resistance of the leaf, R_I, and the external resistance of the boundary layer outside the leaf, R_{BL}, i.e.

$$\dot{N} = \frac{\Delta C}{R_I + R_{BL}} = \frac{\Delta C}{R_T}. \tag{1}$$

If the water vapor in the interior is saturated, it is not difficult to measure the transpiration rate and the driving force experimentally, but in order to isolate the effect of stomatal behavior in the interpretation of the experimental data, it becomes necessary to calculate the magnitude of the external resistance analytically and to assume that no coupling exists between the two resistances [11].

This study was undertaken to develop a theory for predicting the external and internal resistances of a leaf with air flowing over it. A non-living model of a leaf was chosen as the experimental system in order to eliminate the possibility of unknown physiological phenomena affecting the interpretation of the results. In a later phase of this study the results reported here were applied to living leaves [12, 13].

II. EXPERIMENTAL EQUIPMENT AND PROCEDURE

The objective of the experiments was to measure the rate of evaporation from flat plate models of leaves over a wide range of pore geometries and pore densities under flow conditions resembling a natural environment. Most of the evaporation measurements were made in a small ecological wind tunnel (SEWT). This wind tunnel, which is described in more detail by Cannon [14], had provision for temperature, humidity, and irradiation control. In addition to standard instrumentation for measuring air velocity, temperature, humidity, and static pressure, a constant temperature hot wire anemometer was available to measure the turbulence level. Since the turbulence level was rather high in the SEWT, some tests were also made in a large low turbulence level tunnel (LTLT) described by McMichael [15] in order to study the onset, level, and scale of turbulence, and to corroborate the results obtained in the SEWT.

Two groups of plates were used in the experiments (see Table 1). All the plates in the first group, called simulated leaf models, had a high pore density, bracketing conditions found in nature. It would have been desirable to have plates with pore densities between 5×10^5 and 1×10^9 pores/m^2 and with porosities between 2 and 4%, but unfortunately it was not possible to drill or punch sufficiently small holes economically; in addition, Nuclepore Membrane Filters were available in only one size at the time.

All the plates in the other group had a low pore density (about 6000 pores/m^2) and rather large holes. Their physical characteristics do not resemble those of leaves and they were tested mainly because a strange phenomenon, to be described later, was observed and it was hoped that the tests with these plates would shed light on the unexpected observation. All in all, experiments were performed with 13 different perforated plates, having porosities between 0.5 and 5%, pore lengths between 10 μm and 4100 μm, pore densities between 6×10^3 and 9×10^8 pores/m^2, and overall plate dimensions of length in direction of flow and width perpendicular to the flow of 0.127 and 0.0508, 0.203 and 0.0787, and 0.0787 and 0.203 m, respectively. The latter two plate geometries were physically the same plate, but the third was the second plate turned $\pi/2$ radians in the wind tunnel to determine how a change in the L/D ratio would affect the results.

The perforated plate assembly consisted of a holder and a removable perforated plate on top, as shown in Fig. 1. The actual sizes and densities of the

Table 1. Physical characteristics of perforated plates

Plate assembly number	Plate dimension* L/D (m/m)	Pore density (pores/m^2)	Pore diameter, d (μm)	Pore length, t (μm)	t/d	Spacing between pores in flow direction s, (μm)	s/d	Porosity, % open area	Internal resistance R_l (equation 6) (s/m)
				Simulated leaf models					
1	0.203/0.0787	1.00×10^9	8.13	10.9	1.374	31.8	3.9	5.02	9.19
2	0.127/0.0508	1.00×10^9	8.13	10.9	1.374	31.8	3.9	5.02	9.19
3	0.127/0.0508	4.14×10^5	351	130	0.370	1650	4.7	4.00	217
4	0.127/0.0508	2.98×10^5	394	50.8	0.129	2010	5.2	3.62	184
5	0.127/0.0508	1.66×10^5	244	193	0.792	2590	10.6	0.77	1220
6	0.203/0.0787	1.61×10^5	262	208	0.797	2410	9.3	0.86	1160
7	0.0787/0.203	1.61×10^5	262	208	0.797	2410	9.3	0.86	1160
8	0.127/0.0508	9.77×10^4	376	50.8	0.136	2740	7.3	1.08	597
				Low density plate models					
9	0.127/0.0508	6.20×10^3	1090	107	0.099	12700	11.6	0.58	2980
10	0.127/0.0508	5.43×10^3	1060	1740	1.646	14200	13.5	0.48	14600
11	0.127/0.0508	6.20×10^3	1140	4080	3.573	12700	11.1	0.64	22900
12	0.203/0.0787	6.36×10^3	1180	130	0.110	12700	10.8	0.69	2780
13	0.0787/0.203	6.36×10^3	1180	130	0.110	12700	10.8	0.69	2780

*L distance from leading to trailing edge, D width of plate perpendicular to flow direction.

pores in the plates used in this study are presented in Table 1. With the exception of the high density plates (Plate Assemblies Nos. 1 and 2), the perforated plates were made of sheet metal into which precision holes were drilled or punched. The high density plate was a polycarbonate membrane, a product of the General Electric Company called a Nuclepore Membrane Filter. After manufacture, the holes were examined microscopically to verify their exact size and make sure that they were free from burrs. All plate holders and plate assemblies were beveled at the leading edge at an angle of 0.52 radians (30°) to provide a sharp leading edge for the boundary layer.

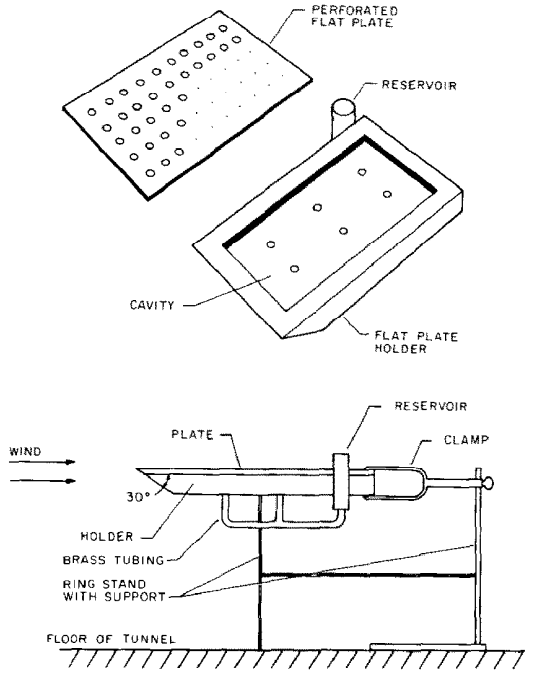

FIG. 1. Experimental model showing plate-holder and perforated plate assembly.

As shown in Fig. 1, water was supplied to the cavity of the plate holder from a small reservoir in its rear, which was connected by a manifold of tubes to the bottom of the cavity. The purpose of the reservoir was to keep the bottom of the cavity saturated with water vapor throughout an experiment as water transpired from the cavity through the perforations during a test. The temperature in the cavity was measured with a thermocouple to verify that conditions remained constant and to evaluate the diffusivity properly. The inside bottom surface of the cavity was lined with blotting paper which was saturated with water before each test. Blotting paper, rather than a free water surface, was used because it was too difficult to handle routinely without spilling an assembly with an open water surface. Initially, however, tests were performed with Plate Assembly No. 5 to ensure that the transpiration rate from a cavity with a free water surface was the same (to within 1%) as that from a cavity lined with blotting paper. The four edges of the perforated plates were sealed to the plate holder before each test run with tape and paraffin wax in order to prevent evaporation anywhere except through perforations on the top. Thus, as shown in more detail in Section III, a perforated plate assembly modeled a transpiring leaf, with the saturated blotting paper taking the place of the outer surface of the mesophyll cells, the gap above simulating the sub-stomatal cavities inside a living plant leaf, and the perforations taking the place of the stomatal passage and opening.

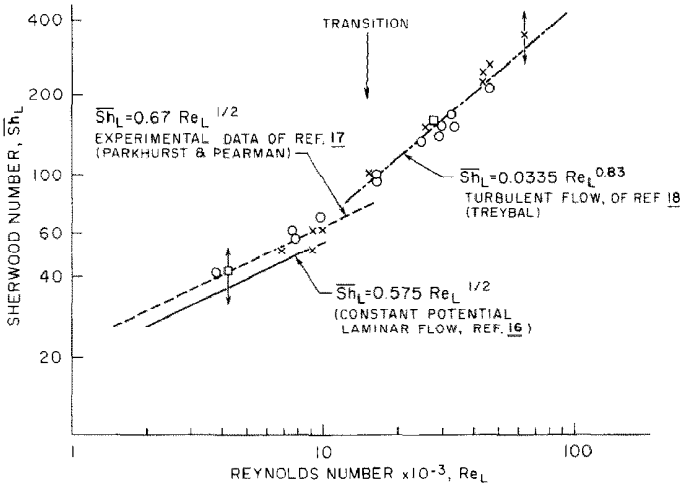

FIG. 2. Calibration data for experimental model—Sherwood number vs Reynolds number for mass transfer from a plate of uniform concentration.

After a plate assembly had been prepared as described, it was placed in the wind tunnel test section, as shown in Fig. 1, where it was held by a clamp at the rear of the plate assembly. The surface of the perforated plate was aligned with a level for tests at zero angle of attack and with a protractor for tests at other angles of attack.

The rate of evaporation through the pores of the perforated plate was determined by weighing the entire assembly periodically at 10–20 min intervals. To obtain the weight of the assembly, it was placed on a Mettler balance, which could be read to within 10^{-5} kg. The balance was located adjacent to the test section, so that a weighing took less than 30 s. The time between weighings was recorded by an automatic timer. During the weighing period the tunnel remained in operation to maintain constant environmental conditions. The first ten minutes of each test were discarded in order for the plate assembly and tunnel to approach equilibrium conditions. Evaporation rates were taken as the differences between consecutive measured weights divided by the time elapsed between weighing. The accuracy of the transpiration rate measurements with the experimental procedure described above is within $\pm 10\%$ [14].

To determine the overall accuracy of the experimental procedure and to ensure that all the equipment was performing properly, an initial series of tests were conducted under conditions similar to those studied previously by other investigators. The system selected for these preliminary tests was a flat plate at uniform concentration and zero angle of attack. The system was constructed by using the same holder which was subsequently used in the simulated leaf studies, but the perforated plate was replaced by a sheet of blotting paper saturated with water to obtain a uniform potential over the entire surface. The holder with the blotting paper was then placed in the wind tunnel and evaporation rates were determined by the same procedure which was used in the simulated leaf model tests.

The experimental mass-transfer data for these tests are shown in Fig. 2 where the average Sherwood number is plotted as a function of the Reynolds number with the distance from the leading to the trailing edge of the blotting paper as the length dimension in both parameters. In the laminar regime the experimental data are compared with predictions from laminar boundary-layer theory [16] as well as with experimental results from convection heat-transfer tests performed in a wind tunnel with a flat plate of 0.0508 m × 0.0762 m surface area [17]. According to boundary-layer theory, the average Sherwood number is related to the Reynolds number by the equation

$$\overline{Sh}_L = 0.575 Re_L^{1/2}, \tag{2}$$

when the Schmidt number is 0.65, the average value for the condition of the tests. Parkhurst and Pearman [17] showed, however, that with a small flat plate in a wind tunnel it is practically impossible to realize the conditions necessary to correspond to the idealized assumptions of laminar boundary-layer theory and that the finite span of the plate causes a slight increase in the coefficient in equation (2). From these heat-transfer experiments it appears that the expected experimental results should lie along the dashed line in Fig. 2, approximately 13% above the line projected by the theory for a plate of infinite span.

According to Treybal [18] the best fit correlation for mass transfer by turbulent forced convection in flow over a flat surface is proportional to $Re^{0.83}$ rather than $Re^{0.80}$ as predicted by Reynolds' analogy. Applying his results, which were obtained in a wetted wall column, to flow over a flat plate with mass transfer of water vapor to air flow above yields the following relation for the average Sherwood number as a function of a Reynolds number for a Schmidt number of 0.65:

$$\overline{Sh}_L = 0.0335 Re_L^{0.83}. \tag{3}$$

Figure 2 shows that in the laminar as well as in the

turbulent flow regime the calibration tests agree with the results of other investigators well within the estimated accuracy of the experimental data. The vertical arrows indicate the range of uncertainty of the experimental values of the Sherwood number at both ends of the Reynolds number range (approximately $\pm 20\%$).

The only unexpected result revealed by the calibration tests was that transition from laminar to turbulent flow begins at a Reynolds number of about 1.5×10^4 rather than 6 or 8×10^4 as predicted by stability theory [19]. This result, however, is in agreement with data obtained by Kestin *et al.* [20], Edwards *et al.* [21], and Grace and Wilson [22] in flow over a flat plate. In these investigations it was found that an increase in turbulence level shifted the transition to a lower Reynolds number, but had no effect on the conventional Nusselt number vs Reynolds number correlation above and below the transition point.

To evaluate the turbulence level in the boundary layer over a plate of the size used in the simulated leaf tests and to determine whether or not the mass-transfer process affects the transition point, a series of tests were also performed in the low turbulence wind tunnel. This tunnel has a free stream turbulence level less than 0.05% at a velocity of 3.05 m/s. The mean velocity and the intensity of the axial component of the turbulence velocity fluctuations were measured at various locations in the boundary layer over the 0.127 m long and 0.0508 m wide plate at free stream velocities between 0.91 and 6.4 m/s both in the presence and absence of transpiration. Measurements were made with a 2.54 μm dia, constant temperature hot wire as described in detail by Cannon [14] and a wave analyzer was used to determine the spectral distribution of the longitudinal turbulence velocity component. These tests show that the turbulence intensity rises sharply at a Reynolds number of 1.5×10^4, indicating that the early transition is primarily a fluid mechanical phenomenon due to the size of the plate and not the result of the high turbulence level in the ecological wind tunnel or the mass transfer from the surface. Similar results were obtained with the 0.203×0.0762 m plate. One may therefore conclude that since the turbulence level above small plates is quite high even at zero angle of attack, the transition at a lower Reynolds number than the value predicted by linear stability theory is not unexpected. Moreover, since high turbulence levels have also been reported by Pearman *et al.* [23] in tests conducted in a natural environment, the experimental results obtained in the ecological wind tunnel correspond to flow conditions expected *in vivo* and the accuracy of the experimental procedure can be considered satisfactory.

III. DEVELOPMENT OF AN ANALYTICAL MODEL

In the development of a mathematical method to predict the rate of transpiration from a model of a real leaf, a compromise between analytical rigor and the degree of complexity must be struck. The model developed in this study takes into account the principal physiological features of a living plant leaf as well as of the external flow field. At the same time, however, to simplify the analysis the model also makes use of experience gained from previous investigations with living plants as well as from flow and heat- and mass-transfer analyses in geometrically similar, but nonliving systems.

Figure 3(a) is a schematic diagram of a typical dicotyledon leaf. It consists of several layers of cells, called the mesophyll, in which photosynthesis occurs. The mesophyll is covered by a layer of different kinds of cells, called the epidermis. The outer wall of the epidermal cells are coated with a waxy substance, called the cutin, which is almost impervious to the diffusion of water vapor. Transport of water from the leaf into the surrounding air occurs through pores, called the stomata. Each stoma is formed by two kidney-shaped cells, called the guard cells, which control the size of the pore opening. According to one widely held theory, since the inner walls of the guard cells are thicker than the outer ones, when the pressure in these cells (the turgor pressure) increases, the weaker outer wall balloons out, carries the inner wall along with it and causes the stomatal pore to open. When the guard cell is flaccid, the thick, elastic inner wall stretches and reduces the pore opening. In this manner plants control their water loss.

When the stoma is open, water passes first from the mesophyll cells into the cavity below the stomatal pore, then in the vapor phase through the stomatal pore to the leaf surface, and finally through the boundary layer over the surface of the leaf into the surrounding air. Although the exact location of the evaporating surface is still a subject of discussion, most plant physiologists agree that it is reasonable to assume that a saturated liquid–vapor interface exists at the outer walls of the mesophyll cells [24, 25]. Unless there is insufficient water in the soil, transpiration can be viewed as a mass-transfer process which, in accordance with the diffusion resistances in the leaf and in the surrounding boundary layer, controls the water consumption of a plant. A quantitative understanding of the energy balance in eco-systems in general and of transpiration in particular requires, therefore, a knowledge of the interaction between the external fluid dynamics and the internal diffusion.

The analytical model for this study is shown schematically in Fig. 3(b). It consists of a perforated plate having the shape of the leaf. Below each perforation is a large cavity, resembling the substomatal cavity, whose surface is saturated with water vapor, intended to resemble conditions at the mesophyll wall. From this interface water vapor diffuses through the boundary layer into the environment.

A problem in modeling the resistance of the system shown in Fig. 3(b) is that the resistance

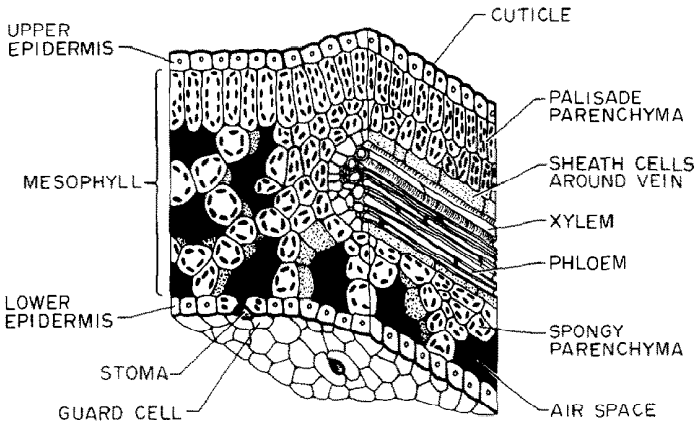

(a)

FIG. 3(a). Cross-sectional diagram of typical leaf.

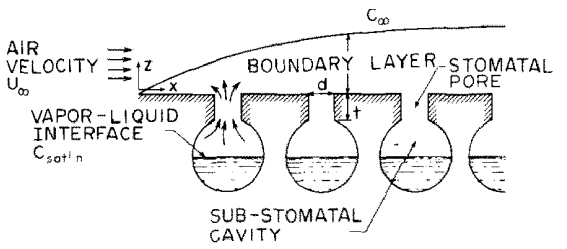

(b)

FIG. 3(b). Schematic sketch for the development of the analytical model for transpiration from a leaf.

associated with the substomatal cavity and stomatal pore is defined only at discrete points along the porous surface, whereas the resistance of the boundary layer is continuous and defined everywhere. The discrete nature of the pore and cavity resistances can be accounted for by determining the pore/cavity resistance per unit area and defining a pore/cavity resistance for every point along the surface.

Transpiration from plant leaves differs from that for the porous flat plates used in this study because all the substomatal cavities are isolated in the former, whereas they are interconnected below the plate in the latter. This interconnection affects the mass-transfer resistance of the cavities, an effect which will be accounted for in a later section, and will be referred to as "interference".

The model studies also account for a second type of interference effect which occurs in the boundary layer and is thus common to leaves as well as porous flat plates. This interference effect arises from the diffusion of the transferring species downstream of the holes. This interference phenomenon in plant leaves, first mentioned by Brown and Escomb [26] at the turn of the 19th century, has been investigated analytically by Weinberg [27]. A proposed rule of thumb is that interference is significant only when the ratio of the distance between pores to the average pore diameter is less than 10. This interference effect, referred to as "boundary-layer interference", was approximated by considering two extreme models. In one, the CIML model (Complete Interference Model Laminar), the interference is assumed to be so effective as to produce a constant concentration along the surface of the porous plate (or leaf). In the other, the NIML model (Non-Interference Model Laminar) it is assumed that the interference is negligible and the surface concentration increases in the direction of flow due to the increase in boundary-layer thickness. Resistance analogies for these two models are shown in Figs. 4(b) and (c), where R_{BL} is the boundary-layer resistance, R_p is the stomatal pore resistance, and R_i is the substomatal cavity resistance. Appropriate equations for these resistances are developed in the subsequent sections.

III.1. *Resistance of a single pore*, R_p

Consider the steady-state unimolecular diffusion of species A in a dilute solution with solvent B. The molar flux of species A through a pore of diameter d and length t is given by

$$\dot{N}_{A_p} = (C_{A_i} - C_{A_o})/R_p = \frac{\Delta C_{A_p}}{R_p} \tag{4}$$

where C_{A_i} and C_{A_o} are the molar concentrations of A at the pore inlet and outlet, respectively, and $R_p = t/\mathscr{D}$ is the resistance of a pore to the mass transport of water vapor, in which $\mathscr{D}$ is the binary diffusion coefficient. The resistance as derived here assumes that the flow in the pore is unidimensional which, for a relatively short pore, is of course an

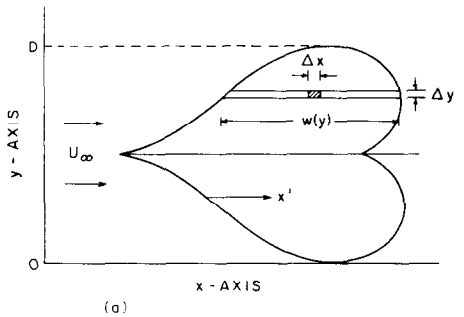

FIG. 4(a). Leaf shape defining $w(y)$.

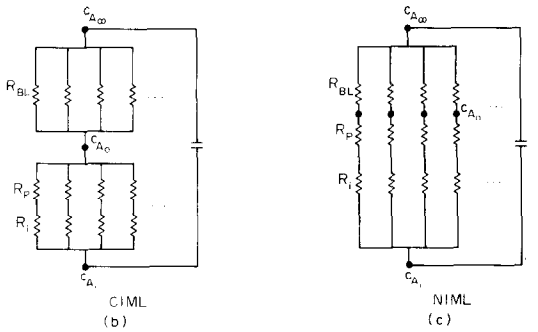

FIG. 4(b), (c). Electric analogs for complete-mixing and no-mixing models.

approximation. The error introduced by this simplification has been investigated [28, 29] and is not serious for the conditions of this study.

III.2. *Inlet resistance of a single pore*

The flux from the substomatal cavity towards a circular opening of a stoma can be calculated by approximating the real system as diffusion from a semi-infinite space towards a circular disk. The molar flow rate can be obtained from the solution to the analogous heat transfer problem given in Carslaw and Jaeger [30]:

$$\dot{N}_{A_p} = \frac{8\mathscr{D}}{\pi d}\Delta C_A. \tag{5}$$

Thus, the inlet resistance for diffusion from the substomatal cavity towards the pore entrance can be approximated by $\pi d/8\mathscr{D}$.

III.3. *Internal resistance of* N *pores without interference*

In the absence of an interference effect due to interconnected pores, the internal resistance offered to diffusion by N pores, R_I, is obtained by combining the inlet resistance and pore resistance for each pore in series. This yields for N pores in parallel

$$R_I = \frac{1}{N}\left(\frac{t}{\mathscr{D}} + \frac{\pi d}{8\mathscr{D}}\right). \tag{6}$$

If the pore diameter is much smaller than the thickness of the boundary layer on the outside in laminar flow, or much smaller than the thickness of the laminar sublayer in turbulent flow, it appears that there may exist an "outlet resistance", similar to the inlet resistance [31].

III.4. *External boundary-layer resistance*

For the water vapor from a substomatal cavity to reach the surrounding atmosphere it must pass through the boundary layer on the outside of the leaf. To obtain the total diffusion resistance it is therefore necessary to incorporate the internal pore resistance as well as the external boundary-layer resistance into the model. While the average internal resistance per unit area depends only on the pore density and geometry, the resistance offered by the boundary layer is a function of the distance from the leading edge and the appropriate functional relationship will depend on whether the flow is laminar or turbulent and whether the convection is free or forced.

4(a) *Forced convection.* In view of the extreme complexity of the physical system, certain simplifying assumptions had to be made in the analysis. The simplest approach is to assume the flow over any section of width dy along the flow direction resembles flow over a flat plate and that the concentration over the entire leaf surface is uniform due to complete and rapid mixing of the water vapor emanating from the pores. This is equivalent to assuming maximum interference between adjacent pores, which effects complete mixing and a uniform surface concentration, and will be referred to as the complete interference or mixing model for laminar boundary-layer flow (CIML). In laminar flow the local Sherwood number at a distance x from the leading edge is

$$Sh_{BL} = \frac{K_{BL}x}{\mathscr{D}} = 0.332\left(\frac{\rho_\infty U_\infty x}{\mu_\infty}\right)^{1/2} Sc^{1/3} \tag{7}$$

whereas the effective average conductance [32] of the boundary layer, $\bar{K}_{BL}$, over a leaf whose shape is defined by a function $w(y)$ as shown in Fig. 4(a) is

$$\bar{K}_{BL} = \frac{\int_0^D \int_0^{w(y)} K_{BL}\,dx'\,dy}{\int_0^D \int_0^{w(y)} dx'\,dy} = 0.664\frac{\mathscr{D}}{L_e} Sc^{1/3}(Re_{L_e})^{1/2}, \tag{8}$$

where x' is a coordinate measured from the local upstream edge of the leaf as shown in Fig. 4(a). The effective length L_e is defined by

$$L_e = \left[\int_0^D w(y)\,dy \Big/ \int_0^D w(y)^{1/2}\,dy\right]^2 \tag{9}$$

for flow over a flat plate of uniform width $L_e = L$, the length of the plate in the direction of flow.

According to equation (1) the total overall resistance for the CIML model for one surface of the leaf model is therefore

$$\bar{R}_T = \frac{1}{\bar{K}_T} = R_I + \bar{R}_{BL}, \tag{10}$$

where $\bar{K}_T = \overline{Sh}_T \mathscr{D}/L_e$. The electrical analog for the CIML model is shown in Fig. 4(b).

A complete interference model can be developed for turbulent flow (CIMT model) if the local Sherwood number is taken from the relation [33]

$$Sh_{BL} = 0.0296 Re_x^{0.8} Sc^{1/3}. \tag{11}$$

One then obtains for the effective average conductance of the boundary layer

$$\bar{K}_{BL} = \frac{1}{\bar{R}_{BL}} = 1.25 \times 0.0296 \frac{\mathscr{D}}{L_e} (Re_{L_e})^{0.8} Sc^{1/3}, \tag{12}$$

where

$$L_e = \left[\int_0^D w(y)\,dy \Big/ \int_0^D w(y)^{0.8}\,dy \right]^5. \tag{13}$$

A model representing another extreme can be obtained if one assumes that there is no mixing in the boundary layer; this is equivalent to assuming no interference between adjacent pores. In this case the concentration at the surface, i.e. at the outlet of the pores, is not uniform because the resistance of the boundary layer varies with distance from the leading edge whereas the internal resistance is the same for all the pores. The relevance of this nonuniformity to actual plant leaves has been discussed in a recent article by Wigley and Clark [34]. The electrical analog for this non-interference model (NIML or no-mixing model) is shown in Fig. 4(c).

Since the concentration, C_{A_O} for the NIML model is not uniform over the surface, the constant in the relation between the Sherwood number and the Reynolds number depends on the functional variation of the concentration which in turn depends on the boundary-layer resistance itself. An accurate solution for the Sherwood number requires therefore numerical methods as shown in [31]. However, since in real leaves most of the diffusion resistance is in the pores, a small error due to a lack of precision in the boundary-layer resistance will not affect the total resistance appreciably. If one assumes that the boundary-layer resistance can be calculated from the available solution for a linearly varying concentration with distance from the leading edge, the overall average mass-transfer coefficient for a perforated surface, $\bar{K}_T$, defined in equation (10) becomes [33]:

$$\bar{K}_T = \int_0^D \int_0^{w(y)} \left(\frac{B}{BR_I + x'^{1/2}} \right) dx'\,dy \Big/ \int_0^L \int_0^D w(y)\,dy\,dx'$$
$$= \frac{\displaystyle\int_0^D 2B \left([w(y)]^{1/2} - BR_I \ln \left\{ 1 + \frac{[w(y)]^{1/2}}{BR_I} \right\} \right) dy}{\displaystyle L \int_0^D w(y)\,dy} \tag{14}$$

where $B = 0.535(\rho_\infty U_\infty / \mu_\infty)^{1/2} \mathscr{D} Sc^{1/3}$.

For flow over a perforated flat plate of constant width D equation (14) reduces to

$$\bar{K}_T = \frac{2B}{L} \left\{ (L)^{1/2} - BR_I \ln \left[1 + \frac{(L)^{1/2}}{BR_I} \right] \right\}. \tag{15}$$

A comparison between the predictions of the complete mixing (CIML) and no-mixing (NIML) models developed here indicates that if the boundary-layer resistance is of comparable magnitude to the internal pore resistance, the effect of boundary-layer interference will be to increase the Sherwood number and hence the evapotranspiration rate. However, if the boundary-layer resistance is considerably less than the internal resistance, the effect of boundary-layer interference will be to decrease the Sherwood number.

4(b). *Free convection.* When the wind velocity is low, the external transport will be by free rather than forced convection. Defining a Grashof number for mass transfer as $Gr_L = (L^3 \rho^2 g/\mu^2)(C_{A_O} - C_{A_\infty})/C_{A_O}$, free convection exists when $Gr_L/Re_L^{2.5}$ is larger than unity. Under these conditions, the boundary-layer resistance must be calculated from appropriate relations for free convection. Only laminar conditions need be considered because turbulent free convection hardly ever exists over a leaf in nature.

For a horizontal flat plate with a higher concentration of water vapor over the top surface than in the surrounding air the average mass-transfer coefficient according to Kreith [35] is

$$\bar{K}_{BL} = \frac{1}{\bar{R}_{BL}} = 0.54(\mathscr{D}/L)(Gr_L \cdot Sc)^{1/4} \tag{16}$$

whereas for the lower surface the coefficient in the above equation becomes 0.27.

According to equation (16), the boundary-layer resistance is a function of the surface concentration in the Grashof number. For the complete mixing model, the surface concentration can be calculated since the rate of mass transfer from the cavity equals the rate of mass transfer from the surface, or

$$\dot{N}_A = \frac{(C_{A_i} - C_{A_O})}{R_I} = \frac{(C_{A_O} - C_{A_\infty})}{\bar{R}_{BL}}. \tag{17}$$

Substituting equation (16) for $\bar{R}_{BL}$ gives

$$\frac{(C_{A_i} - C_{A_O})}{R_I} = \frac{C_{A_O} - C_{A_\infty}}{W[C_{A_O}/(C_{A_O} - C_{A_\infty})]^{1/4}} \tag{18}$$

where $W = [0.54(\mathscr{D}/L)(L^3 \rho^2 g/\mu^2 \mathscr{D})^{1/4}]^{-1}$ for the upper surface. Equation (18) can be solved for C_{A_O} by iteration and the result substituted in equation (16) to obtain the resistance of the free convection boundary layer and in equation (10) to calculate the total rate of mass transfer from the cavity into the surrounding air. Combined free and forced convection occurs when $(Gr_L/Re_L^{2.5})$ is between 0.1 and 1.0 [36].

III.5. *Interference resistance*

The CIML and NIML models provide bounds on the effect of boundary-layer interference arising from diffusion of the transferring species downstream of the holes. The interference effect arising from the

interconnected substomatal cavities in the porous flat plates used in this study will be considered next.

The interference effect of interest here is related to a problem solved by Keller and Stein [37]. These investigators solved the Fourier equation for a matrix of pores with diffusion into a stagnant boundary layer on one side, assuming that the pores are equally spaced so that water vapor from each pore could diffuse only into a hexagonal space in the stagnant layer. In the mathematical treatment they replaced this hexagonal cylinder by a circular cylinder of diameter $2b$, the average distance between the axes of adjacent pores. For a stagnant boundary layer of thickness, δ, with equally spaced pores of radius a, the diffusion resistance can be expressed in the form

$$R_l = (4a/\mathscr{D})4.7\phi(\beta, \lambda), \tag{19}$$

where

$$\phi(\beta,\lambda)=\frac{\lambda}{4\beta^2}+\frac{1}{\beta^2}\sum_{n=1}^{\infty}\frac{J_1^2(\alpha_n a)\tanh(\alpha_n a\lambda)}{(\alpha_n a)^3 J_0^2(\alpha_n a\beta)}, \tag{20}$$

with $\beta = b/a$, $\lambda = \delta/\alpha$, and (α_n) obtained from $J_1(\alpha_n\beta) = 0$.

The interference effect considered by Keller and Stein is found to be negligible for ratios of pore spacing to diameter larger than 10 if λ is less than 20, but the effect can become appreciable for larger spacing to diameter ratios if the stagnant layer is thick, i.e. λ is large. Since the analysis of Keller and Stein ignores any motion in the boundary layer, it is not quantitatively applicable to the outer surface over which the boundary layer flows and where it would indicate unrealistically large resistances. The analysis of Keller and Stein does, however, have an important bearing on the application of the experimental results with a perforated plate to a real leaf. Since it was practically impossible to provide each pore in the perforated plate of the experimental model with a source of its own, there is a difference between the experimental model and the analytical model describing a leaf. In the experimental model the water vapor diffused from a sheet of blotting paper at uniform potential towards and through the pores, whereas in a leaf, as well as in the analytical model describing a leaf, each pore is fed by its own sub-stomatal cavity. Consequently, there exists in the experimental model an entry interference when the pores are closely spaced. This effect, which is significant for some of the high density plate assemblies, must therefore be taken into account in the comparison of the experimental results with the predictions from the analytical leaf model. However, since the conditions at the inlet to the pores, i.e. between the upper surface of the sheet of blotting paper and the lower surface of the perforated plate, correspond exactly to the system described by Keller and Stein, the Sherwood number for a perforated plate assembly can be corrected for interference effects at the inlet of the pores by multiplying the inlet resistance for an isolated pore in equation (6) by the interference factor 4.7ϕ. In the interpretation of the experiments to be discussed in the following section, the theoretical predictions corrected for inlet pore interference effects are referred to as "with interference". In all cases where this correction was applied, δ was assumed equal to 1590 μm.

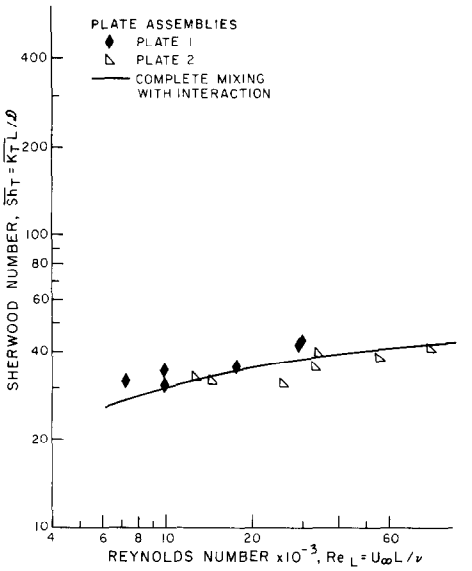

FIG. 5. Sherwood number vs Reynolds number for plate assemblies Nos. 1 and 2 (high density, stoma-sized pores – see Table 1 for dimensions of plates and pores).

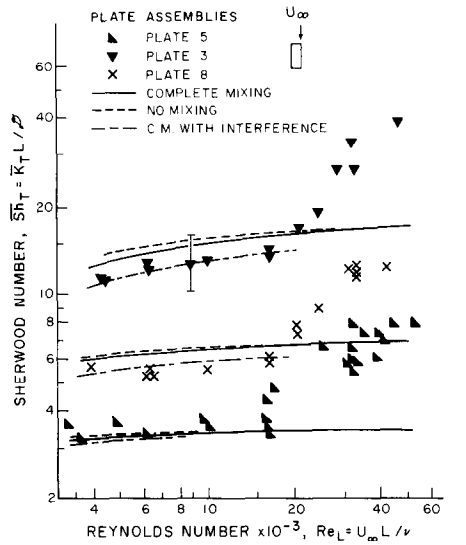

FIG. 6. Sherwood number vs Reynolds number for plate assemblies Nos. 3, 5 and 8 (see Table 1 for physical dimensions of plates and pores).

IV. EXPERIMENTAL RESULTS

Typical experimental results for evaporation from plate assemblies 1, 2, 3, 5 and 8 are shown in Figs. 5 and 6 where the overall Sherwood number for each configuration ($\overline{Sh}_T = \dot{m}L/\mathscr{D}A_t\Delta C$) is plotted as a function of the plate Reynolds number (Re_L

$= \rho_\infty U_\infty L/\mu$). The legends in these figures relate the symbols for each plate and pore configuration to the physical dimensions given in Table 1. All the data in Figs. 5 and 6 were taken at zero angle of attack, the physical properties of the water vapor used in the reduction of the data were based on the temperature in the cavity as measured by a thermocouple, whereas the properties of the air in the free stream, as well as its velocity, were taken at the average value in the test section. The results for the other plate assemblies are given in the thesis of Cannon [14].

A few tests were made at a Reynolds number of 3.2×10^4 to determine the effect of the angle of attack of the surface of the plate on the evaporation rate. The results of these tests are compared in Table 2 for a surface of uniform concentration, as well as for a perforated plate, with the results of tests at zero angle of attack. When the leading edge is tilted upward the transpiration rate is larger than for a horizontal surface, whereas downward tilting of the leading edge reduces the rate of evaporation. The net rate of increase is qualitatively in agreement with results obtained by Parkhurst and Pearman [17] in convective heat transfer from a leaf model, where an angle of attack of 0.14 rad (8°) increased the total rate of heat transfer from both surfaces by 30%.

Table 2. Comparison of evaporation rates from horizontal flat surfaces and flat surfaces at small angles of inclination to the wind

Angle of inclination,* (radians)	$r.h._\infty$	T_∞ (K)	T_c (K)	$Re_L \times 10^{-3}$	$\Delta\rho \times 10^2$ (kg/m^3)	$\dot{m} \times 10^7$ (kg/s)	$\overline{Sh}_T = \dot{m}L/A_t\Delta\rho\mathscr{D}$
Evaporation from a plate with uniform concentration ($L/W = 2.5$)							
−0.175	0.191	299.8	292.0	31.943	1.13	28.50	169.1
0	0.213	299.0	292.2	32.359	1.12	25.18	127.6
+0.175	0.210	299.9	294.1	31.799	1.29	21.25	109.4
Evaporation from plate assembly No. 5							
−0.175	0.209	299.2	297.1	32.033	1.66	3.278	13.10
−0.0873	0.198	299.9	298.6	32.265	1.86	2.056	7.38
0	0.266	299.7	298.7	31.841	1.71	1.519	5.84
0	0.209	299.2	298.2	32.033	1.80	1.519	5.56
+0.0873	0.264	299.8	299.2	32.096	1.77	1.028	3.84
+0.175	0.266	299.7	299.0	31.840	1.75	1.074	4.04

* Positive angles indicate that leading edge of plate is tilted down, whereas negative angles indicate that leading edge of plate is tilted up.

Figure 5 shows the Sherwood number vs Reynolds number for plates 1 and 2. These are the high pore density plates made of Nuclepore membranes. The solid line in this figure corresponds to the predictions of equation (8), the complete mixing model, corrected for inlet pore interference effects using equation (19). The agreement over the entire Reynolds number range between the data and the model is within the experimental accuracy estimated by Cannon [14] to be ±20%. These data do not show any detectable effects from laminar to turbulent boundary-layer transition. Transition did occur, however, at Reynolds numbers of approximately 1.5×10^4, but had no noticeable effect on the measured Sherwood numbers because for these extremely small pores the mass transfer was entirely controlled by the internal pore resistance. For this reason the Nuclepore membrane data provide no test of the ability of the models for describing the external boundary-layer resistance to diffusional transfer.

Figure 6 compares the predictions of the complete mixing (equation 8), no-mixing (equation 15), and complete mixing corrected for inlet pore interference effects (using equation 19) models with the data for plates 3, 8, and 5, given in order of increasing pore spacing-to-diameter ratio. The difference between predictions of the complete mixing and no-mixing models is seen to be rather insignificant except for plate 3. This result is reasonable since the boundary-layer interference effect which is accounted for in the complete mixing model, but totally ignored in the no-mixing model, should be most pronounced for plate 3 because of its relatively small pore spacing-to-diameter (s/d) ratio. Again the correction for inlet pore interference effects is seen to be significant for these data.

In contrast to Fig. 5, the experimentally measured Sherwood number in Fig. 6 begins to rise abruptly at a Reynolds number of approximately 15000 and reaches a value two to three times larger than that predicted by any of equations 8, 12, or 15 at a Reynolds number of 45000. A similar phenomenon was observed in the data for plates 4, 6, and 7 (not shown). This enhanced rate of evapotranspiration is considerably greater than would be predicted by the turbulent boundary-layer model; hence the predictions of this model are not shown in Fig. 6.

Initially, it was believed that this unexpected enhancement in the rate of evaporation could be the result of the decrease in the boundary-layer resistance accompanying the transition from laminar

to turbulent flow which occurs approximately at the same Reynolds number as the change in shape of the Sherwood number–Reynolds number correlation curve. However, the increase in the experimental Sherwood number is so large that even if one were to assume that the boundary layer offers no resistance at all and calculate a Sherwood number based only on the internal resistance within the pores, the model still could not quantitatively explain the observed values in the "enhanced" transpiration region. The Sherwood number increase in the "enhanced" transpiration region therefore cannot be explained within the framework of the original model, but must be the result of an unexpected new phenomenon which had heretofore not been taken into account in the analysis. The absence of this "enhanced" transpiration region in the Nuclepore membrane studies strongly suggests that the phenomenon is due to altered transport in larger pores. At this point of the investigation four general hypotheses were advanced to explain the observed increased in Sherwood number:

1. An additional interference phenomenon between pores could change the flow pattern in the pores.
2. A pressure gradient due to the shear over the plate surface could induce a flow into the cavity near the leading edge and outward through pores near the trailing edge.
3. A pressure gradient in the boundary layer perpendicular to the plate surface could induce a convective flow of substantial magnitude through the pores.
4. Turbulent eddies from the zone of maximum generation could penetrate into the pores.

In order to test the first hypothesis, several plates of similar porosity but with larger pores were constructed in order to eliminate the possibility that some type of unexpected interaction phenomenon between pores could influence the evapotranspiration; this has often been used by plant physiologists as an *ad hoc* theory to explain unexpectedly large water losses observed occasionally with living plants [38–42]. The results of experiments with several plates having a porosity of about 0.5%, relatively large and widely spaced holes, are shown in Fig. 7 where the total Sherwood number is plotted as a function of Reynolds number. The lines in this figure represent a least squares fit of the data rather than theoretical predictions. One observes again the existence of an "enhanced" evaporation region at Reynolds numbers above 15000. These results, as well as the higher than predicted transpiration rates observed by Ting and Loomis [41, 42] even with a single pore membrane in a wind velocity of about 5.18 m/s, indicate that interference between pores cannot be responsible for the "enhancing" mechanism which produces the unexpected increases in Sherwood number.

The second and third hypotheses were tested by examining how the pore geometry affects the

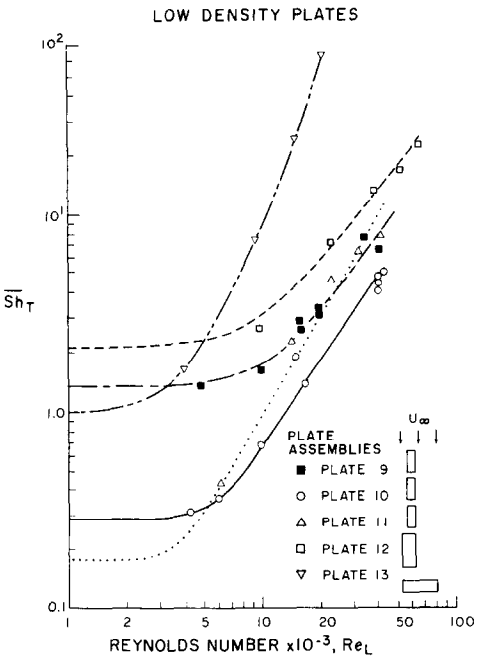

FIG. 7. Sherwood number vs Reynolds number for low density plate models, plates 9, 10, 11, 12, 13 (see Table 1 for physical dimensions of plates and pores).

transpiration in the enhanced regime. The ratio of the experimental to the predicted Sherwood number at a Reynolds number of 4.5×10^4 was plotted vs the pore diameter for plate assemblies Nos. 3, 5, 6, 9, and 12 which have nearly the same pore diameter. These plots established that the degree of enhancement increases both with pore length and pore diameter. The dependence of the degree of enhancement on the ratio of pore length to diameter was also examined, however, no correlation could be found.

If the flow mechanism postulated under our second hypothesis were responsible for the enhancement in transpiration, one would not expect the degree of enhancement to increase with an increase in pore length, since this would retard the flow both into and out of the cavity. Furthermore, hypothesis No. 2 would imply that enhancement would be observed only with multiple pores. Yet, Edwards and Furber [21] observed enhancement with a single pore. Thus, this hypothesis was abandoned.

The results in Figs. 6 and 7 and the geometry effects discussed above suggest that a mechanism to account for the enhanced transpiration regime would have to commence at the transition Reynolds number and exert proportionally more influence as the Reynolds number, pore diameter, and pore length increase. The mechanism suggested under hypothesis No. 3 would be able to provide for an increase in transpiration with increasing Reynolds number and pore diameter, but not with pore length. Nevertheless, the maximum bulk flow that could occur through the pores due to a pressure difference between the cavity and the surface of the plate was determined analytically by Cannon [14]. Although

the predicted bulk flow was directionally correct, the pressure difference across the boundary layer was an order of magnitude too small to account for the observed transpiration rates.

These consistently reproducible experimental results which were not in agreement with predictions based on conventional transport processes thus made it necessary to examine a fundamentally new type of mechanism. Numerical calculations by Ruchal, Spalding and Wolfshein [43] for the steady transport of heat and mass in a two-dimensional square cavity have shown that in two-dimensional flow over a square cavity, mass penetration by recirculating eddies can occur even at creeping flow Reynolds numbers, and that it is possible for turbulence to penetrate into such cavities provided that the scale of the turbulence is of the same order of magnitude as the cavity opening. Although these calculations were made only for two-dimensional systems, they suggested a qualitative direction for examining a three-dimensional system such as the pores in the plates used in the experiments.

V. A TURBULENT PENETRATION THEORY

As shown in the body of this article, the experimentally measured Sherwood number for mass transfer through a perforated plate, emanating from a large source located below the plate, into an air stream flowing above the plate, begins to rise abruptly at a Reynolds number of about 15000 when the size of the perforations is above some critical size. The onset of this phenomenon occurs simultaneously with transition from laminar to turbulent flow in the boundary layer above the plate. However, the increase in the measured overall mass transfer coefficient is much larger than can be accounted for by the change in boundary-layer resistance due to transition from laminar to turbulent flow. Of the four hypotheses to explain these observations, three had to be rejected either because they could not account for the observations quantitatively or because they were in qualitative disagreement with the trends of one or more of the governing parameters. The analysis presented below constitutes the fourth hypothesis. Although additional experiments will be necessary to test this hypothesis, the mechanism postulated here can account for the experimental results.

The mechanism of mass transfer in the "enhanced regime" is a combination of diffusion and turbulent transport. Under normal transport conditions mass is transferred from the source in accordance with Fick's law into and through each pore by diffusion and by turbulent convection from the outlet of the pore into the boundary layer. Periodically, however, the laminar sublayer above the pores is penetrated by turbulent eddies which sweep into the holes, remove the air and water vapor in the holes and replace the mixture by air from the boundary layer. In this manner, the diffusional transport through the pores is augmented by a convective transport which is far more effective than ordinary diffusion and can transfer mass from the pores at a much higher rate than is predicted by Fick's law. This mechanism can operate only when the hole size is equal to or larger than the microscale of the turbulence in the flow.

Assuming that the RMS velocity fluctuations perpendicular to the wall bring fresh air from the mean flow into the pores and at the same time remove the air and water vapor residing previously within the pores, the mass transfer flux from a single pore by the eddy penetration mechanism is

$$\dot{N} = v' f \Delta C. \tag{21}$$

The RMS velocity fluctuation v' in the vicinity of a wall has been correlated empirically with the turbulent energy e by the relation [44–46]

$$\overline{vv} \simeq 0.27e. \tag{22}$$

The turbulent energy, in turn, is related to the Reynolds stress in the wall region by

$$\overline{uv} \simeq -0.20e. \tag{23}$$

Near the wall the Reynolds stress reaches a maximum value characterized by

$$\overline{uv} \simeq -v^{*2}, \tag{24}$$

where $v^* = (\tau_w/\rho)^{1/2}$ is the friction velocity which can be evaluated from available correlations between the wall shear τ_w, and free stream velocity U_∞ [16]:

$$\tau_w/\rho = 0.0296 U_\infty^2 (Re_x)^{-0.2}. \tag{25}$$

The symbol f in equation (21) denotes the penetration coefficient. Physically it can be interpreted as a parameter whose value depends on the percentage of eddies which penetrate into the pores, the depth to which the eddies penetrate, the effectiveness with which eddies exchange gas and vapor within the pores, and the concentration gradient existing under normal diffusion conditions within the pores. The penetration coefficient should be a function of the spectral energy distribution in the vicinity of the wall, the Schmidt number, and the pore Reynolds number. For the proposed penetration model to be physically viable, the coefficient f must be less than unity.

Combining equations (21)–(25) yields the following equation for the mass-transfer coefficient for a single pore via turbulent penetration:

$$K_{TP} = 0.2 f U_\infty Re_x^{-0.1}. \tag{26}$$

The turbulent penetration mechanism described above in general will operate alternately with ordinary diffusion through the pores due to the random nature of eddy penetration. However, it will be assumed here that ordinary diffusion contributes relatively little to the total mass transfer and thus can be neglected. However, one cannot ignore the mass-transfer resistance offered by the turbulent boundary layer. The local Sherwood number for turbulent boundary-layer flow is given by equation (11). Again we can combine these mass-transfer

resistances via either a complete mixing or no-mixing model corresponding to Figs. 4(b) and (c), respectively. We will combine these resistances via the complete mixing model since the additional sophistication of the no-mixing model is unwarranted at this point. Furthermore, since the pore resistance is predominant relative to the resistance of the turbulent boundary layer, there should be relatively little difference between the predictions of the complete and no-mixing models.

The Sherwood number corresponding to the average mass-transfer coefficient for turbulent penetration in the pores is then given by

$$\overline{Sh}_{TP} = 0.222Sc(Re_L)^{0.9} f(N \cdot A_p/A_t), \quad (27)$$

where N is the number of pores, A_p is the area of a single pore, and A_t is the total area of the plate. The Sherwood number corresponding to the average mass-transfer coefficient for turbulent boundary-layer flow is given by

$$\overline{Sh}_L = 0.037(Sc)^{1/3}(Re_L)^{0.8}. \quad (28)$$

The overall Sherwood number for the turbulent enhancement mechanism based on the complete interference model is then

$$\overline{Sh}_E = \overline{Sh}_{TP}\overline{Sh}_L/(\overline{Sh}_{TP} + \overline{Sh}_L). \quad (29)$$

The turbulent penetration model is consistent with the observed effect of the pore geometry on the enhancement. This can be seen by comparing the ratio of the Sherwood number for turbulent penetration to that corresponding to ordinary diffusion in the pores, which is related to the pore resistance defined by equation (6):

$$\frac{\overline{Sh}_{TP}}{\overline{Sh}_I} = \frac{0.222(t + \pi d/8)Sc(Re_L)^{0.9} f(NA_p/A_t)}{NL}. \quad (30)$$

The above implies that the degree of enhancement will increase both with pore length t and pore diameter d; recall here that both A_p and f are proportional to the pore diameter as well.

In order to test the validity of the penetration model to explain the mass transfer mechanism in the enhancement region and to analyze data in that region, the experimental results for plate assemblies 4, 8, 9, and 12 were analyzed in the following manner. The Sherwood number for the turbulent penetration was obtained from equation (29) using the experimentally determined overall Sherwood number and $\overline{Sh}_L$ from equation (28). The penetration factor f was then determined from equation (27). The penetration factors for these plates were determined at a Reynolds number of 40 000 since one would expect penetration factors of similar magnitude at a given Reynolds number for these plates if the turbulent penetration model is viable. In all cases the Schmidt number was assumed to be 0.65, the average value for all the tests.

As shown in Table 3, at a Reynolds number of 40 000 the penetration factors for plate assemblies 4, 8, 9, and 12 are 0.67, 0.71, 0.88, and 1.07, respectively. The latter penetration factor is not significantly different from unity in view of the experimental accuracy of $\pm 20\%$ for the measured overall Sherwood numbers. Thus, these estimates of the penetration factors indicate that the proposed eddy penetration model is reasonable. In addition, qualitative observations by Professor Wiganski at Tel Aviv University [47] have confirmed the existence of eddy penetration. As a final argument in support of the turbulence penetration hypothesis proposed here, it should be noted that the measured microscale of the turbulence was 914 μm; the effects of the penetration mechanism were not observed with pores of diameter considerably smaller than this value as can be seen from Fig. 5. However, since the typical microscale of atmospheric turbulence is considerably larger than the characteristic dimensions of stomata, it is doubtful that the penetration mechanism is operative in real plant leaves.

Table 3. Determination of penetration factors for $Re_L = 40\,000$

Plate assembly No. →	4	8	9	12
Pore diameter, d	394 μm	376 μm	1090 μm	1180 μm
Porosity, $100NA_p/A_t$	3.62	1.08	0.58	0.69
Sherwood No., $\overline{Sh}_E$	37.0	14.0	9.6	13.5
$\overline{Sh}_L$	154	154	154	154
$\overline{Sh}_{TP}$	48.7	15.4	10.2	14.8
f	0.67	0.71	0.88	1.07

CONCLUSIONS AND RECOMMENDATIONS

1. Analytical models were developed to predict the transpiration through perforated plates simulating the stomata of dicotyledon leaves under various flow conditions. The rate of mass transfer predicted by means of the analysis agreed with experimental data obtained in an ecological wind tunnel in laminar boundary-layer flow over the plates to within $\pm 20\%$ over a range of pore diameters between 7.62 and 1170 μm and pore lengths between 50.8 and 4060 μm.

2. For rectangular shaped plates ranging from 0.0508–0.203 m in length and length to diameter ratios between 0.4 and 2.5, transition from laminar to turbulent flow occurs in the boundary layer at

Reynolds numbers based on the length of the plate of about 1.5×10^5; this transition is independent of transpiration.

3. In the turbulent flow regime the experimentally observed transpiration rates were considerably higher than those predicted by the analytical model based upon diffusion theory within the pores and turbulent boundary layer outside the pores when the pore diameter is larger than the microscale of the turbulence in the boundary layer. This increase in transpiration rates in the turbulent flow regime was explained by means of an eddy penetration model.

4. Positive angles of inclination to the wind (i.e. leading edge of plate tilted down) yielded smaller transpiration rates from the upper surface than were observed for horizontal plates whereas negative angles of inclination yielded larger transpiration rates than those observed for horizontal plates.

5. The penetration model used to explain the enhanced transpiration rate at high Reynolds numbers should be investigated in more detail and the turbulence spectrum of the penetrating eddies should be measured.

6. The analytical model should be modified to account for the internal pore structure of living plants and calculations based on the actual shape of the internal pores should be compared with transpiration rates from living plants and ecosystems under controlled environmental conditions in order to predict the effectiveness of chemical antitranspirants of the stomata-closing types.

Acknowledgements—The authors gratefully acknowledge financial assistance by the National Science Foundation under Grant No. GK 17184, The Office of Water Resource Technology under Project C-6030CAL, by the Council on Research and Creative Work of the University of Colorado, by the Office of Water Resource Research (Pre-Doctoral Fellowships to Dr. J. Cannon), and the University of the Negev. The authors are also grateful to Professor F. Ramirez of the University of Colorado, Professor D. B. Spalding and Dr. A. K. Runchal of the Imperial College of Science and Technology, and to Professor M. Wolfshein of the Technion for helpful discussion in the developmental stage of the penetration model, and Professor W. Wignanski of Tel Aviv University for making some preliminary measurements verifying the existence of penetrating eddies. They also wish to thank Dr. A. Taori for helpful suggestions in the final draft of the manuscript.

REFERENCES

1. R. Russell-Scott and D. A. Barber, The relationship between salt uptake and the absorption of water by intact plants, *A. Rev. Pl. Physiol.* **11**, 127 (1960).
2. J. Gale and R. M. Hagan, Plant antitranspirants, *A. Rev. Pl. Physiol.* **17**, 269 (1966).
3. I. Zelitch and P. E. Waggoner, Effect of chemical control of stomata on transpiration of intact plants, *Proc. Natn. Acad. Sci. U.S.* **48**, 1297 (1962).
4. P. E. Waggoner, J. L. Monteith and G. Szeicz, Decreasing transpiration of field plants by chemical closure of stomata, *Nature (London)* **201**, 97 (1964).
5. R. O. Slatyer and J. F. Bierhuizen, The influences of several transpiration suppressants on transpiration, photosynthesis, and water-use efficiency of cotton leaves, *Aust. J. Biol. Sci.* **17**, 131 (1964).
6. D. Mishra and G. C. Pradhan, Effects of transpiration reducing chemicals on growth, flowering, and stomatal opening of tomato plants, *Pl. Physiol.* **50**, 271–274 (1972).
7. H. J. Ketellapper, Stomatal physiology, *A. Rev. Pl. Physiol.* **14**, 249–270 (1963).
8. H. Meidner and T. A. Mansfield, *Physiology of Stomata*. McGraw-Hill, New York (1968).
9. A. Poljakoff-Mayber and J. Gale, Physiological basis and practical problems of reducing transpiration, in *Water Deficit and Plant Growth*, Vol. 3, Chapter 9. Academic Press, New York (1972).
10. P. Gaastra, Photosynthesis of crop plants as influenced by light, carbon dioxide, temperature and stomatal diffusion resistance, *Meded. LandbHoogesch. Wageningen* **59**, 1–68 (1959).
11. J. L. Monteith, *Principles of Environmental Physics*. Edward Arnold, London (1973).
12. A. Taori, Mathematical modelling of transpiration from leaves, Ph.D. Thesis, University of Colorado (1973).
13. F. Kreith and A. Taori, The use of antitranspirants to control water consumption in ecosystems, in *Heat and Mass Transfer in the Biosphere*, Vol. 1, pp. 489–500, edited by D. A. de Vries and N. H. Afgan. Scripta, Washington (1975).
14. J. N. Cannon, A model study of transpiration from broad leaves, Ph.D. Thesis, University of Colorado (1971).
15. J. McMichael, A study of the axisymmetric turbulent wake generated by co-flowing incompressible streams, Ph.D. Thesis, University of Colorado (1971).
16. H. Schlichting, *Boundary Layer Theory*, 6th edn. McGraw-Hill, New York (1968).
17. D. F. Parkhurst and G. I. Pearman, Convective heat transfer from a semi-infinite, flat-plate leaf model to periodic flow in a wind tunnel, First Australian Conference on Heat- and Mass-Transfer, Monash University, Melbourne, Australia (Preprint) (May 1973).
18. R. E. Treybal, *Mass Transfer Operations*. McGraw-Hill, New York (1955).
19. C. C. Lin, *The Theory of Hydrodynamic Stability*. Cambridge University Press, London (1970).
20. J. Kestin, P. F. Naeder and H. E. Wong, Influence of turbulence on the transfer of heat from plates with and without a pressure gradient, *Int. J. Heat Mass Transfer* **3**, 133–154 (1961).
21. A. Edwards and B. N. Furber, The influence of free-stream turbulence on the transfer of heat from plates with and without a pressure gradient, *Proc. Instn Mech. Engrs* **170**, 941 (1956).
22. J. Grace and J. Wilson, The boundary layer over a populus leaf, *J. Exp. Bot.* **27**(97), 231 (1976).
23. G. I. Pearman, H. L. Weaver and C. B. Tanner, Boundary layer heat transfer coefficients under field conditions, *Agric. Meteorol.* **10**, 83–91 (1972).
24. T. T. Kozlowski (editor), *Water Deficits and Plant Growth, Development, Control and Measurement*, Vol. 2. Academic Press, New York (1968).
25. R. O. Slatyer, *Plant–Water Relationships*. Academic Press, New York (1967).
26. H. T. Brown and F. Escomb, Static diffusion of gases and liquids in relation to the assimilation of carbon and translocation in plants, *Phil. Trans. R. Soc.* **193B**, 223–291 (1900).
27. B. C. Weinberg, Mass transfer from plates with finite sources: predictions of the influence of pore spacing on evapotranspiration, *Mech. Engrs*. Tokyo, Japan (1974).
28. S. S. Rao and C. O. Bennett, Radial effects in a Stefan diffusion tube, *IEC Fundamentals* **5**(4), 573–575 (1966).
29. F. J. Heinzelmann, D. T. Wasan and C. R. Wilke, Concentration profiles in a Stefan diffusion tube, *IEC Fundamentals* **4**(1), 55–61 (1965).
30. H. S. Carslaw and J. C. Jaeger, *Conduction of Heat in*

Solids, 2nd edn. Oxford University Press, London (1959).
31. B. C. Weinberg and F. Kreith, Evapotranspiration from a plate with finite sources, in *Proceedings of the 5th International Heat Transfer Conference*. Tokyo (1974).
32. D. F. Parkhurst, P. R. Duncan, D. M. Gates and F. Kreith, Wind tunnel modelling of convection of heat between air and broad leaves of plants, *Agric. Meteorol.* **5**, 33–47 (1968).
33. W. M. Kays, *Convective Heat and Mass Transfer*. McGraw-Hill, New York (1966).
34. G. Wigley and J. A. Clark, Heat transport coefficients for constant energy flux models of broad leaves, *Boundary-Layer Meteorol.* **7**, 139 (1974).
35. F. Kreith, *Principles of Heat Transfer*, 3rd edn. Int. Textbook Co., New York (1973).
36. Y. Mori, Buoyancy effects in forced laminar convection flow over a horizontal flat plate, *J. Heat Transfer* **83**, 479–482 (1961).
37. H. K. Keller and T. R. Stein, A two-dimensional analysis of porous membrane transport, *Math. Biol. Sci.* **1**, 421–437 (1967).
38. P. E. Miller and D. M. Gates, Transpiration resistance of plants, *Am. Midl. Nat.* **77**, 77 (1967).
39. B. Huber, Untersuchung uber die Gesetze der Porenverdunftung, *Z. Bot.* **23**, 839 (1930).
40. G. G. J. Bange, On the quantitative explanation of stomatal transpiration, *Acta. Bot. Neerl.* **23**, 255 (1953).
41. I. P. Ting, and W. E. Loomis, Diffusion through stomates, *Am. J. Bot.* **50**, 866 (1963).
42. I. P. Ting and W. E. Loomis, Further studies concerning stomatal diffusion, *Pl. Physiol.* **40**, 220 (1965).
43. A. K. Ruchal, D. B. Spalding and M. Wolfshein, Numerical solution of the elliptic equations for transport of vorticity, heat, and matter in two-dimensional flow, *Physics Fluids Suppl.* II, *High Speed Comp. in Fluid Dyn.* **21** (1969).
44. J. A. Clar, Study of incompressible turbulent boundary-layer in a two-dimensional wind tunnel, Ph.D. Thesis, Queen's University of Belfast (1966).
45. G. Comte-Bellot and P. de A. Craya, Ecoulement turbulent entre deux parois paralleles, Pub. Sci. et Tech. du Ministers de L'air, No. 419 (1965).
46. J. Laufer, Investigation of turbulent flow in a two-dimensional channel, NACA Rept. No. 1053 (1951).
47. M. Wignanski, University of Tel Aviv, Israel, Private Communication (1973).

ETUDE DE LA TRANSPIRATION DE PLAQUES PLANES POREUSES SIMULANT DES FEUILLES DE PLANTES

Résumé—L'article présente des modèles analytiques pour prédire la transpiration à travers des plaques perforées qui simulent les stomates de feuilles de dicotylédon pour des conditions d'écoulement variées et il compare les calculs avec des résultats expérimentaux. L'analyse est basée sur des concepts fondamentaux de la théorie de couche limite et du transfert convectif de chaleur et de masse. Les expériences sont conduites dans une soufflerie écologique avec des plaques perforées de géométrie correspondant à de larges feuilles. Des anomalies imprévues dans les résultats sont expliquées à l'aide d'une théorie de pénétration turbulente.

EINE UNTERSUCHUNG DER TRANSPIRATION VON PORÖSEN, EBENEN PLATTEN ZUR SIMULATION VON PFLANZENBLÄTTERN

Zusammenfassung—Dieser Artikel gibt analytische Modelle zur Voraussage der Transpiration durch perforierte Blätter wieder. Die Poren von Blattkeimer-Blättern werden unter verschiedenen Strömungsbedingungen simuliert und die analytischen Voraussagen mit experimentellen Ergebnissen verglichen. Die Berechnung basiert auf fundamentalen Vorstellungen der Grenzschichttheorie und des Wärme- und Stoffübergangs. Die Versuche wurden in einem ökologischen Windkanal mit perforierten Platten, die der Porengeometrie breiter Blätter ähnlich sind, durchgeführt. Einige unerwartete Anomalien in den Ergebnissen werden mit Hilfe einer turbulenten Penetrationstheorie erklärt.

ИССЛЕДОВАНИЕ ИСПАРЕНИЯ ИЗ ПЛОСКИХ ПОРИСТЫХ ПЛАСТИН, МОДЕЛИРУЮЩИХ ЛИСТЬЯ РАСТЕНИЙ

Аннотация — В статье рассматриваются аналитические модели, описывающие транспирацию через перфорированные пластины, моделирующие листья двудольных растений с устьицами при различных условиях обтекания. Проводится сравнение теоретических результатов с экспериментальными данными. Анализ основывается на фундаментальных понятиях теории пограничного слоя и конвективного тепло- и массообмена. Эксперименты проводились в экологической аэродинамической трубе с пластинами, перфорированными в виде устьиц широких листьев. Ряд непредвиденных аномалий в результатах объяснен с помощью теории турбулентного проникновения.